Advanced Materials Research *Online: 2014-08-11*
ISSN: 1662-8985, Vol. 996, pp 848-854
doi:10.4028/www.scientific.net/AMR.996.848

Investigations on thermal stresses of a graded Ti(C,N) coating deposited on WC-Co hardmetal

E. Ramos-Moore[1,a*], C. Espinoza[1,b], R.S. Coelho[2,c], H. Pinto[3,d], P. Brito[4,e], F. Soldera[5,f], F. Mücklich[5,g] and J. Garcia[6,h]

[1]Facultad de Física, Pontificia Universidad Católica de Chile, Santiago 7820436, Chile.

[2]Helmholtz-Zentrum Berlin für Materialien und Energie GmbH, Albert-Einstein-Str. 15 12489, Berlin, Germay

[3]Universidade de São Paulo, Av. Trabalhador São Carlense 400, 13566-590 São Carlos SP, Brazil.

[4]Pontifícia Universidade Católica de Minas Gerais, Av. Dom José Gaspar 500, 30535-901 Belo Horizonte MG, Brazil.

[5]Universität des Saarlandes, Functional Materials, Campus D3.3, D-66123 Saarbrücken, Germany.

[6]Sandvik Machining Solutions, R&D Materials & Processeses, Lerkrogsvägen 19, SE 12160 Stockholm, Sweden.

[a]evramos@fis.puc.cl, [b]cfespinoza@uc.cl, [c]rodrigo.coelho@helmholtz-berlin.de, [d]haroldo@sc.usp.br, [e]pbrito@pucminas.br, [f]f.soldera@matsci.uni-sb.de,

[g]muecke@matsci.uni-sb.de, [h]jose.garcia@sandvik.com

* Corresponding author

Keywords: CVD coatings, cemented carbides, Ti(C,N) coatings, synchrotron radiation, thermal stress.

Abstract. We investigated the stress behaviour of Ti(C,N) coatings deposited on WC-Co substrates during an individual thermal cycle. The stress analyses were performed in-situ by energy dispersive X-ray diffraction using a white synchrotron beam. The stresses were determined using the $\sin^2\psi$ method combined with scattering vector measurements at the strain-free ψ-tilt, in order to avoid the effect of the chemical C/N gradient on the strain distributions over $\sin^2\psi$. It was found that compressive stresses induced by top blasting on the coating are released after the individual thermal cycle. During heating and cooling, part of the Ti(C,N) coating was oxidized into a TiO_2 rutile phase. Stress analysis was also performed in this phase in order to evaluate the influence of oxidation on the residual stress of the coating. The obtained results can support the design of coated tools with improved properties at interrupted cutting operations by understanding the role of thermal cycling on the stresses of Ti(C,N) coatings.

1. Introduction

Cutting tools are often subjected to strong load and heat impacts during machining operations [1]. In order to enhance their wear resistance, hard coatings based on TiN, or combinations such as TiN-TiCN-Al_2O_3 and TiAlN, are deposited by chemical and/or physical vapour deposition methods [2]. Mismatches of the Coefficient of Thermal Expansion (CTE) between the coating and the cemented carbide substrate may lead to the development of thermal stresses under interrupted cutting conditions, which may accelerate the formation and propagation of cracks and failures [3]. Surface post-treatments of coated inserts such as brushing or blasting are state-of-the-art. In particular, top-blasting is used to introduce compressive stresses in the top-layer of the coating systems as well as to reduce its roughness, leading to an overall improvement of the cutting tool

performance [4]. However, so far in-situ studies focused on quantifying stress development in hard coatings under thermal cycling conditions have not been performed intensively.

In this work we investigated the evolution of thermal stresses in Ti(C,N) coatings deposited on cemented WC-Co inserts in as-coated and blasted conditions. The Ti(C,N) layers were produced by a modified CVD process, which generates chemical gradients within the coating [5]. The effect of thermal cycling on the stress state of Ti(C,N) was evaluated in-situ using Energy Dispersive (ED) X-ray diffraction (XRD). Scattering vector analysis [6] was applied in order to avoid the influence of the chemical composition gradient on the strain distributions over $\sin^2\psi$. The influence of Ti oxidation on the residual stresses present in the Ti(C,N) coating after the thermal cycling was quantified by performing the $\sin^2\psi$ method in the TiO_2 rutile phase.

2. Experimental Methods

Sample Description. Cemented carbide substrates made of WC (90%) and Co (10%) were produced by conventional powder metallurgy techniques, including mixing of raw powders, pressing, dewaxing and sintering at liquid phase temperatures (1450 ºC /1h). These substrates were coated in a CVD-hot-wall reactor in a second step with multilayer TiN/Ti(C,N) thin films. A thin protective TiN layer was first deposited at 850 ºC followed by the Ti(C,N) coating deposited by a modified CVD-process in which the temperature increases (900 ºC - 1050 ºC) at a constant rate during the process [5]. Fig. 1 presents Scanning Electron Microscopy (SEM) micrographs and optical micrographs of the analysed sample. The CVD fabrication induces a chemical gradient that was characterized by an electron probe micro-analyser (EPMA). As presented in the right image of Fig. 1, the C/N ratio obtained by EPMA increases exponentially with the coating depth. . After deposition, some coatings were subjected to blasting treatment using Al_2O_3 slurry.

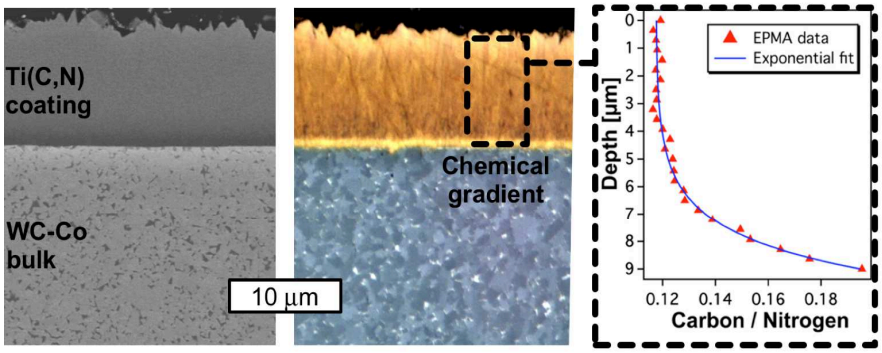

Figure 1. SEM (left) and optical (middle) micrographs of the Ti(C,N) coating - WC substrate system in the as-coated condition. The EPMA data of the coating layer (right) shows the exponential increase of the C/N ratio as a function of the coating depth.

Electron Backscattered Diffraction (EBSD) was performed in the coating system in order to evaluate the presence of texture in the Ti(C,N) phase. In Fig. 2, the inverse pole figure map and 220, 111 and 200 pole figures are presented (these reflections are used posteriorly for stress analysis). As shown in the inverse pole figure map, no strong preferential orientation is present in the coating. Pole figures show a weak (texture strength ~2) 110 preferential orientation in the normal direction, which should not negatively affect the ED-XRD stress measurements.

X-ray Diffraction Analysis. Synchrotron XRD experiments were performed applying the ED method at the material science beam line EDDI (Energy-Dispersive Diffraction) located in the BESSY storage ring of the Helmholtz-Zentrum Berlin, Germany [7]. ED diffraction relies upon a polychromatic X-ray beam, which allows for the acquisition of complete energy resolved diffraction spectra at a fixed detector position (2θ). In the ED spectrum, each diffraction line (hkl) stems from a certain energy (E^{hkl}) level, which can in turn be related to the lattice distance (d^{hkl}) via Bragg's law, as described in Eq. 1.

$$E^{hkl}\left[keV\right] = \frac{0.6199}{\sin\theta} \cdot \frac{1}{d^{hkl}\left[\text{nm}\right]} \tag{1}$$

In the present study, 2θ was kept fixed at 10° and the stress calculations were performed by applying the $\sin^2\psi$ method. The primary beam cross-section was set to 0.5 × 0.5 mm^2 and the $\sin^2\psi$ data were obtained in the symmetrical ψ-mode using $\sin^2\psi$-steps of 0.1. A total of 10 ψ positions were chosen and an exposure time of 30 s per diffractogram was employed. Thus, one single stress measurement took around 5 min. The diffraction elastic constants (DEC) of Ti(C,N) were calculated by means of the Eshelby-Kröner model using the single crystal elastic constants, as treated by Klaus et al. [8]. In ED diffraction, each reflection originates from a certain energy level and corresponds, therefore, to a specific penetration depth τ^{hkl}, which can be calculated by Eq. 2, following the description by Genzel [9], where μ is the absorption coefficient that depends on the reflection energy (E^{hkl}) and η the sample rotation around the scattering vector.

$$\tau^{hkl} = \frac{\sin^2\theta - \sin^2\psi + \cos^2\theta \sin^2\psi \sin^2\eta}{2\mu\left(E^{hkl}\right)\sin\theta\cos\psi} \tag{2}$$

Owing to the C/N-gradient existing in the Ti(C,N) coatings investigated, the unstrained lattice spacing d_0^{hkl} becomes also a function of τ^{hkl}. As a result, the determination of the biaxial coating stresses (σ_ϕ) requires the determination of the influences of the chemical composition on the ε^{hkl}-$\sin^2\psi$ distributions. This was accomplished by determining the exponentially weighted $d_0^{hkl}(\tau^{hkl})$-gradients through independent scattering vector measurements at the strain-free ψ*-tilt at both room temperature and 800° C. Further methods information can be found in [10]. Since Ti(C,N) exhibits a quasi-isotropic mechanical response, ψ* is approximately the same (34.5°) for all <hkl> lattice directions. Based on the EPMA data of Fig. 1, it is expected that the μ and DEC values might change with the coating depth. Nevertheless, for stress calculations, the DEC values were assumed to be constant, neglecting also the influence of the temperature.

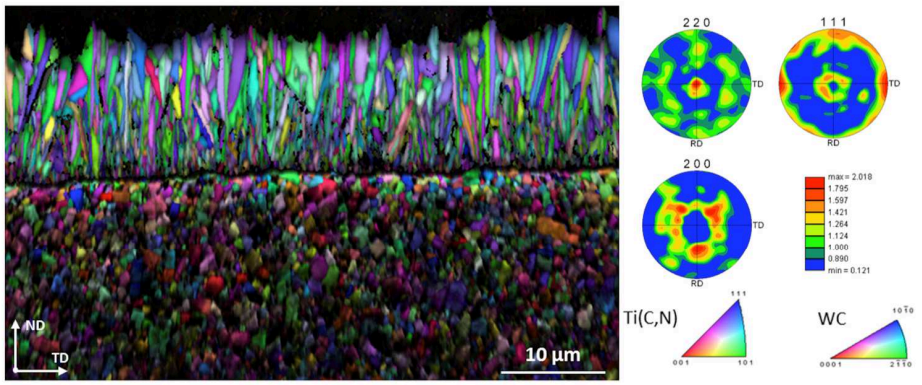

Figure 2. Inverse pole figure map of the Ti(C,N) and WC phases and pole figures of the Ti(C,N) reflections 220, 111 and 200 used to evaluate the stress in the coating layer. The measurements were performed on the sample in the as-coated condition.

The analysis of the thermal influence on the residual stress behaviour for each material was conducted in-situ using an Anton Paar resistance furnace, which allowed for the stabilization of the desired temperature in approximately 10 min. The individual thermal cycle was performed in three steps: room temperature (25° C) before heating; high temperature (800° C); and room temperature after heating. The averaged heating and cooling rates were around 70 ºC/min and 35 ºC/min, respectively.

3. Results and Discussion

Scattering Vector and $\sin^2\psi$ Analysis. A sample ED spectrum acquired at room temperature before the thermal cycle is presented in Fig. 3. Measurements were performed at two different ψ positions corresponding to high (ψ = 0°) and low (ψ = 72°) penetration depths. In this case, the shift of the Ti(C,N) reflections produced a strain of around 0.03%. As shown in Fig. 3, the 111, 200, and 220 reflections of the Ti(C,N) phase are distinguished from the peak reflections of the substrate phases WC and Co.

The distributions of d_0^{hkl}-spacings of Ti(C,N) as a function of the penetration depth, which were measured in the scattering vector mode during the η rotation, show a strongly nonlinear dependence (see Fig. 4A). This measurement was performed on the as-coated sample before the thermal cycling. No significant difference was observed in the data when comparing with blasted samples or samples heated at 800 ºC. Fig. 4B shows data analyses. The chemical gradient leads to a lattice expansion towards the Ti(C,N)/cemented carbide interface due to the increasing C content. It is worth to note that the effect of the TiN protective layer is neglected due to its reduced thickness (0.5 µm). Accordingly the strain-free lattice spacing increases with increasing η and τ^{hkl}. For this analysis, the penetration depths were determined based on the energy of the diffraction line as well on the angles ψ and η according to Eq. 2. Assuming a linear relationship between the lattice parameter and the C and N concentrations of the Ti(C,N) coatings , i.e. the Vegard's law, the depth dependence of the unstrained lattice spacing $d_0^{hkl}(\tau^{hkl})$ obtained through the scattering vector method can be described by Eq. 3, where *D* is the coating thickness and the terms a_0 and a_1 are fitting parameters.

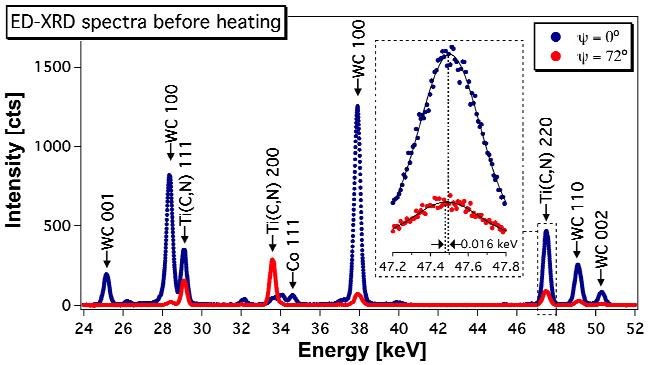

Figure 3: ED spectra of the coating system before thermal cycling measured at room temperature in two different ψ positions.

$$d_0^{hkl}\left(\tau^{hkl}\right) = a_0 + a_1 \cdot \left[\tau^{hkl} + \frac{D}{1-\exp\left(D/\tau^{hkl}\right)}\right] \quad (3)$$

As shown in Fig. 4B, Eq.3 was least squares fitted to the experimental $d_0^{hkl}(\tau^{hkl})$-depth profiles obtained from Eq.2 to enable the correction of each ε^{hkl}-$\sin^2\psi$ distribution with respect to the chemical gradient in the coatings. As an example, Fig. 5A shows corrected ε^{hkl}-$\sin^2\psi$ plots of the Ti(C,N) coating measured at room temperature, before heating. After correcting the ε^{hkl}- $\sin^2\psi$ distributions with respect to the chemical d_0^{hkl}-gradient, the $\sin^2\psi$ curves from the different diffraction lines exhibit similar slope values, indicating the absence of stress gradients within the range of penetration depth. Thus, in order to obtain more representative stress values, the stress determination was accomplished by a weighted averaging of the $\sin^2\psi$ curves from the diffraction lines using their corresponding multiplicity factors. In this case, the stress determination required the averaging of the lattice strains in the 111, 200 and 220 directions, as shown in the $\langle\varepsilon^{hkl}\rangle$-$\sin^2\psi$ plots of Fig. 5B. As can be noted in the ED spectra of Fig. 3, there is a strong convolution of peaks around the 200 Ti(C,N) for low ψ angles due to the high beam penetration. Therefore, only data with ψ > 25º was taken into account for this reflection, as presented in Fig. 5. The as-coated sample

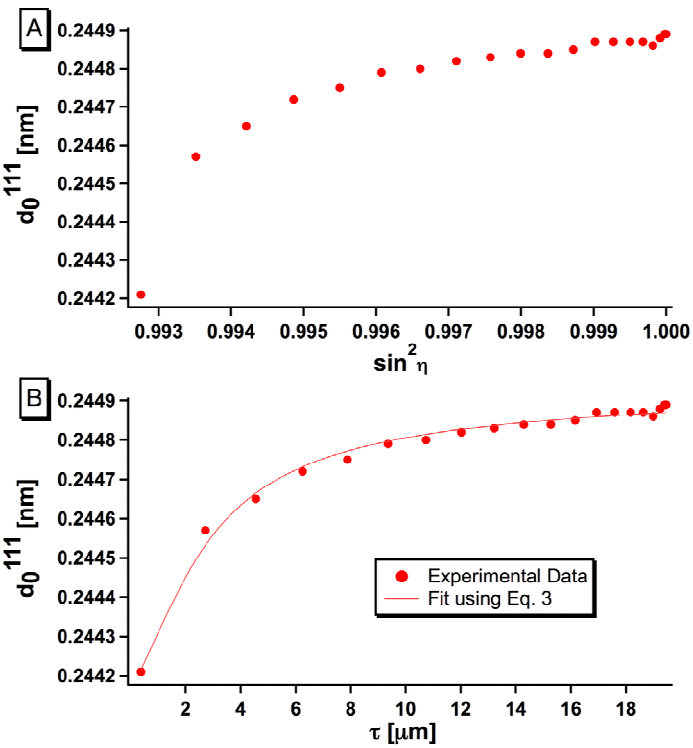

Figure 4. A) d_0^{111}-spacing measured through the scattering vector method before the thermal cycle at room temperature on the as-coated sample. B) $d_0^{111}(\tau^{111})$-depth profiles obtained from applying Eq. 2 on the data in A.

measured at high temperature shows a stress of -435 ± 45 MPa, which is produced by the CTE mismatch (Δα) between Ti(C,N) (8.5×10^{-6} K^{-1})[11] and WC–Co (5.5×10^{-6} K^{-1})[1], and thus can be roughly estimated as $\sigma = -E_{TiN} \cdot \Delta\alpha \cdot \Delta T \approx -584$ MPa, using the Young modulus of TiN ($E_{TiN} = 251$ GPa). Both theoretical and experimental values agree within 25% of accuracy error. This difference may arise mainly due to the presence of cracks, which in general releases stresses. The residual stresses during the thermal cycling are summarized in Fig. 7. It is worth to note that the compressive stress induced by blasting is relieved after the thermal cycle.

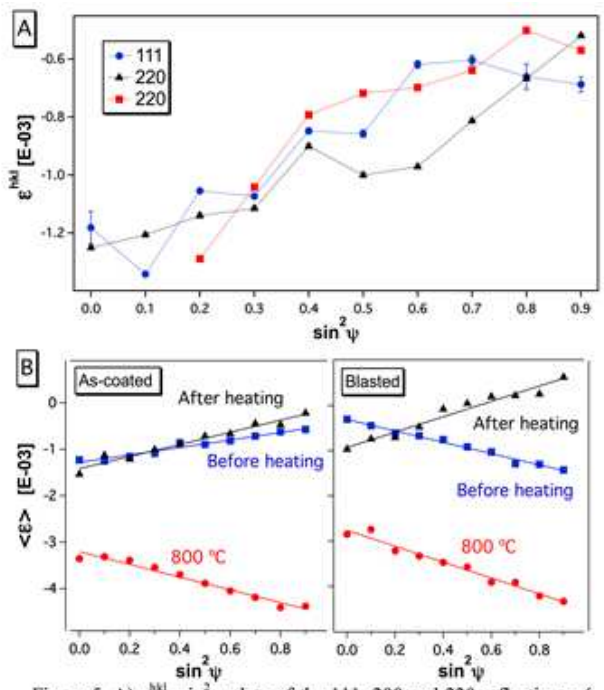

Figure 5. A) ε^{hkl}- $\sin^2\psi$ plots of the 111, 200 and 220 reflections of the Ti(C,N) phase measured before the thermal cycle at room temperature on the as-coated sample. B) Thermal evolution of $<\varepsilon^{hkl}>$-$\sin^2\psi$ plots accomplished by a weighted averaging of the $\sin^2\psi$ curves from the 111, 200 and 220 diffraction lines.

Coating Oxidation. The thermal cycle caused the oxidation of the Ti(C,N) coating during about 20 min, considering heating and cooling. Fig. 6A shows the ED spectra of a sample before and after the thermal cycle. After heating, the oxidation of Ti(C,N) is evidenced in the diffractograms and also in the optical micrographs as a grey layer on top of the Ti(C,N) coating. The residual stresses in the TiO_2 layer was estimated by weight averaging each single stress value calculated through linear regression of the ε^{hkl}-$\sin^2\psi$ distributions measured in the 200, 210, 111, 211 and 220 reflections. As an example, Fig. 6B shows the $\sin^2\psi$ plot of the 210 reflection of TiO_2 at room temperature after heating. The thermal evolution of the stress in the oxide layer is difficult to measure, since the oxidation occurred while measuring at high temperature also. As shown in Fig. 7, compressive stresses are found in the TiO_2 layer in the blasted samples and the tensile residual stresses of the Ti(C,N) layer after cooling are higher than the initial condition. These preliminary results may indicate that the formation of the oxide layer could affect the stress intensity of the TiCN layer at different temperature levels. Moreover, the oxide layer might also undergo cracking during cooling back to room temperature. The effect of oxidation of the TiCN layer and formation of the Ti-oxide layer on the stress and cutting performance of multilayer systems will be studied in future works".

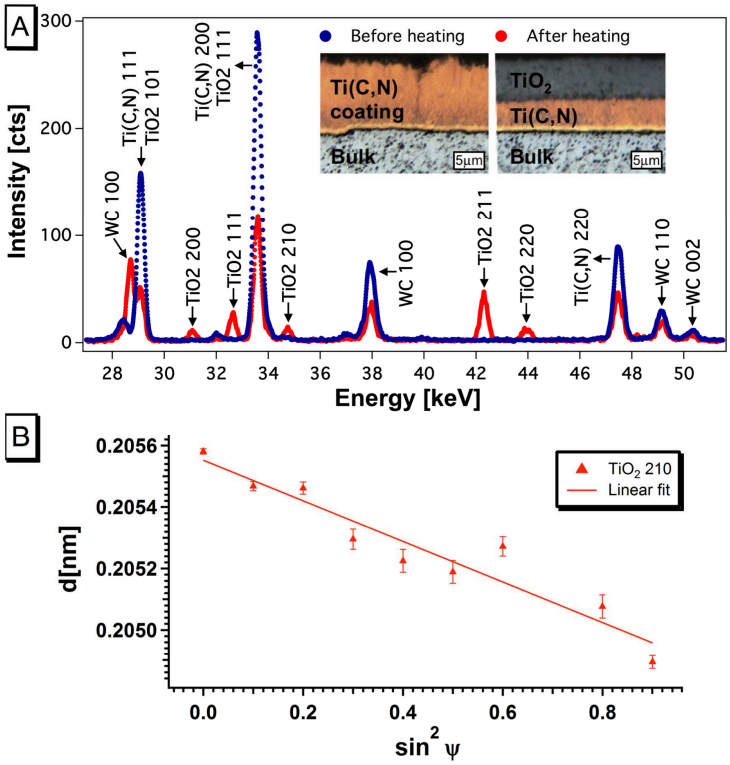

Figure 6: A) ED-XRD spectra of the coating system before and after the thermal cycling. After heating, the oxidation of Ti was evidenced in the spectrum and also in the optical micrograph (insert). B) $\sin^2\psi$ plot of the 210 reflection of TiO_2 rutile phase at room temperature, after heating.

4. Conclusions

The stress behaviour of Ti(C,N) coatings deposited on cemented WC-Co substrates was investigated by ED-XRD in-situ during an individual thermal cycle. The residual and thermal stresses were determined using the $\sin^2\psi$ method combined to scattering vector measurements in order to consider the effect of the compositional gradient in the coating. The compressive stress induced by blasting is shown to relieve after the first thermal cycle, whereas the oxidation of Ti produce a TiO_2 rutile layer that may affect the stress behaviour of Ti(C,N) coatings under working conditions.

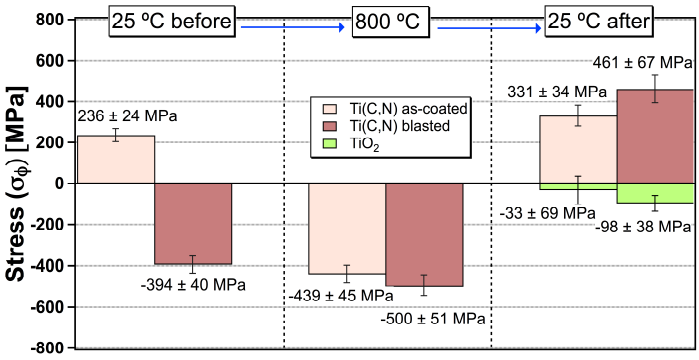

Acknowledgements

E. Ramos-Moore thanks the financial support from the project Fondecyt 11121630, Chile. H. Pinto acknowledges the funding of FAPESP (Process 2010/11391-2). F. Soldera and F. Mücklich thank the EFRE (AME-Lab project) and IRSES (Project N° 318903) funds of the European Commission.

References

[1] K.J.A. Brookes, World Directory and Handbook of Hardmetals And Hard Materials, sixth ed., International Carbide Data, 1996.

[2] H.E. Rebenne, D.G. Bhat, Review of CVD TiN coatings for wear-resistant applications: deposition processes, properties and performance, Surf. Coat. Tech. 63 (1994) 1-13.

[3] Modern Metal Cutting: A Practical Handbook, Sandvik Coromant, first ed., S.O.M. Engineers, 1996.

[4] C. Barbatti, J. Garcia, R. Pitonak, H. Pinto, A. Kostka, A. Di Prinzio, M.H. Staia, A.R. Pyzalla, Influence of micro-blasting on the microstructure and residual stresses of CVD κ-Al2O3 coatings, Surf. Coat. Tech. 203 (2009) 3708–3717.

[5] J. Garcia, R. Pitonak, R. Weissenbacher, A. Köpf, Production and characterization of wear resistant Ti(C,N) coatings manufactured by modified chemical vapor deposition process, Surf. Coat.Tech. 205 (2010) 2322–2327.

[6] C. Genzel, A self-consistent method for X-ray diffraction analysis of multiaxial residual-stress fields in the near-surface region of polycrystalline materials. I. Theoretical concept, J. Appl. Crystallogr. 32 (1999) 770–778.

[7] C. Genzel, I.A. Denks, J. Gibmeier, M. Klaus, G. Wagener, The materials science synchrotron beamline EDDI for energy-dispersive diffraction analysis, Nucl. Instrum. Meth. 578 (2007) 23-33.

[8] M. Klaus, C. Genzel, H. Holzschuh, Residual stress depth profiling in complex hard coating systems by X-ray diffraction, Thin Solid Films 517 (2008) 1172–1176.

[9] C. Genzel, Formalism for the evaluation of strongly non-linear surface stress fields by X-ray diffraction performed in the scattering vector mode, Phys. Status Solidi A. 146 (1994) 629–637.

[10] J. Garcia, R. Coelho, E. Ramos-Moore, H. Pinto, In-situ stress analysis of graded TiCN coating during thermal cycling: submitted to Int. J. Refractory Metals and Hard Mater. (2014).

[11] C. Friedrich, G. Berg, E. Broszeit, C. Berger, Datensammlung zu Hartstoffeigenschaften, Mat.-Wiss. U. Werkstofftech. 28 (1997) 59–76.